

## Surface Crystalline Modification for Asymmetric Giant Magnetoimpedance Profile in Annealed Co-based Amorphous Ribbons

Y. W. Rheem<sup>1</sup>, C. G. Kim<sup>1</sup>, C. O. Kim<sup>1</sup> and Y. Choi<sup>2</sup>

<sup>1</sup>Department of Materials Engineering, Chungnam National University, Taejeon 305-764, Korea

<sup>2</sup>Department of Materials Engineering, Sun Moon University, Chungnam 336-840, Korea

(Received 7 June 2001)

Microstructure modifications are investigated for annealed Co-based amorphous ribbon in vacuum and open air. X-ray diffraction (XRD) spectra for annealed sample in vacuum indicate atomic arrangements with initial nucleation of hcp-Co crystallite at 380 °C annealing temperature. However, the XRD spectra in samples with long annealing times of  $t_a \geq 300$  min demonstrate sharp and good developed surface crystalline hcp-, fcc-Co and Co<sub>2</sub>Si phases. The giant magnetoimpedance (GMI) profile at 0.1 MHz displaying one-peak behavior in vacuum annealed samples at  $T = 380$  °C, irrespective of annealing time  $t_a$  from 20 to 480 min. For the annealed samples in an open air, the GMI profile shows two-peaks for  $t_a = 20$  min annealed sample. However, one of peaks disappears and an asymmetric GMI profile exhibits a drastic step-like change near zero field for  $t_a \geq 300$  min. Such asymmetric GMI characteristics is related to the surface microstructures of fcc-Co, hcp-Co and Co<sub>2</sub>Si crystalline phases.

**Key words :** Co-based amorphous, giant magnetoimpedance, magneto-optic, surface crystalline

### 1. Introduction

Much work has been done on the giant magnetoimpedance (GMI) in soft magnetic Co-based amorphous wires and ribbons because of the high potential for magnetic sensor applications [1-3]. GMI is the effect of a magnetic field on the transverse permeability in the direction of the ac measuring current. The sensitivity and linearity for the magnetic field are the most important parameters in the practical application of GMI. The asymmetric GMI profile, showing GMI-valve phenomenon with a high field sensitivity and linearity, has been realized by field-annealing of Co-based amorphous ribbon in open air [4,5]. However, there is no detail analysis for the microcrystalline structures of surface and bulk materials according to annealing environment, affecting the GMI profiles.

It is well known, that optical and magneto-optical spectra depend strongly on microstructure modifications [6,7], which take place in surface layer during treatments; therefore magneto-optical approach can give possibilities to control and analyze them.

In this work, amorphous Co<sub>66</sub>Fe<sub>4</sub>B<sub>15</sub>Si<sub>15</sub> ribbons were annealed at a temperature of 380 °C at various annealing time both in vacuum and in open air, and their microstructures

have been examined by magneto-optical spectra and X-ray diffraction analysis. The purpose of doing so is to analyze the surface crystalline transformations and to clarify its relation to measured GMI behaviour.

### 2. Experiment

Amorphous ribbons of Co<sub>66</sub>Fe<sub>4</sub>B<sub>15</sub>Si<sub>15</sub> were annealed at temperature  $T_a = 380$  °C for various annealing time ( $t_a$ ) in vacuum (A-batch), and in open air (B-batch). The field of 3 Oe was applied during the annealing of both A- and B-batch samples, where the direction of annealing field was regarded as positive.

The magneto-optical properties were investigated with the analysis of the transverse Kerr effect (TKE) spectra. Measurements were made with the automated equipment by the dynamic method. The spectra were measured in an energy range from 1.5 to 4.5 eV at room temperature.

X-ray diffraction experiments were done by GID method (grazing incidence diffraction) using Philips diffractometer type X'Pert-MPD with Cu-target ( $\lambda_{Cu} = 0.154184$  nm).  $2\theta$ -scans were performed in order to check the surface crystallization.

The impedance  $Z$  was measured by using a HP4192A impedance analyzer with four terminal contacts. The amplitude of the ac current was kept at a constant value of 5 mA during the sweep of the applied field,  $H$ . The GMI ratio

\*Tel: +82-42-821-6229, e-mail: cgkim@cnu.ac.kr

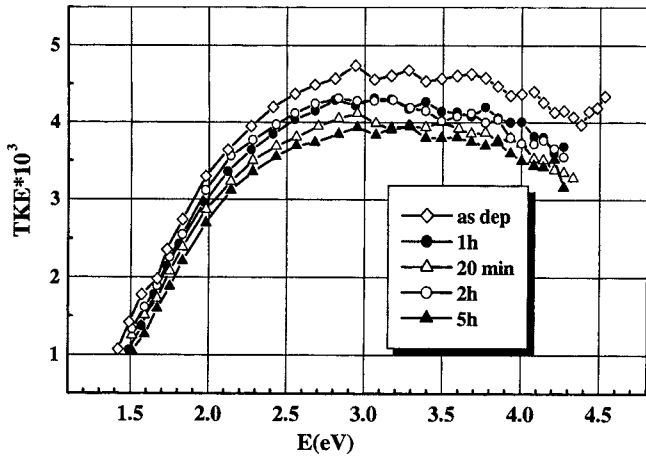


Fig. 1. The TKE spectra for the samples annealed at 380 °C in vacuum (A-batch) for various times at 2 Oe annealing field.

profile was obtained by plotting  $\Delta Z/Z(\%) = (Z(H) - Z_{sat})/Z_{sat} \times 100$  for the cyclic applied field, where  $Z_{sat}$  was the impedance at  $H = 16$  Oe.

### 3. Results and Discussion

Fig. 1 shows the magneto-optical properties of TKE spectra for A-batch samples. It is seen that the shape of the TKE spectra does not change with the increase in the annealing time and is typical for amorphous alloys [6,7]. Consequently the crystalline phase did not appear in the samples

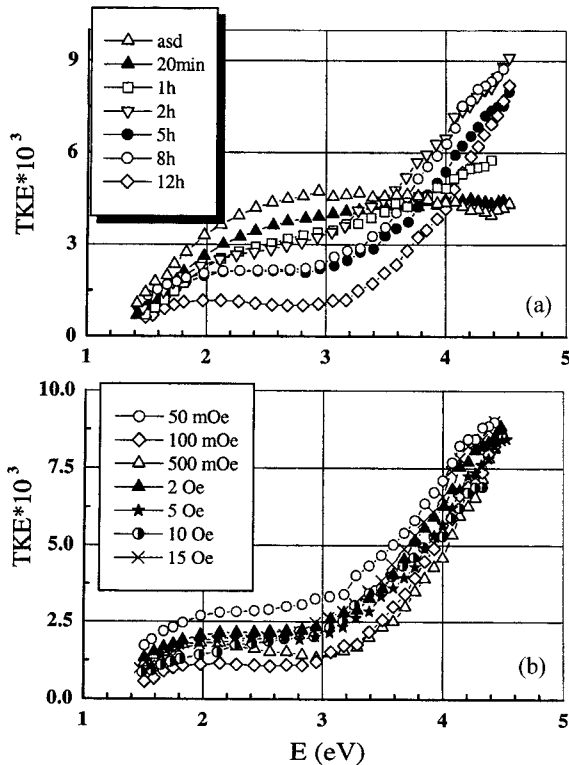


Fig. 2. The TKE spectra for the samples annealed at 380 °C in air (B-batch). (a) - samples annealed at 2 Oe for various times. (b) - samples annealed for 8 hours in different fields.

annealed in vacuum. Also, changes in magnetostatic properties were not found for this sample at the time of annealing up to 36 hours.

The investigation of the magneto-optical properties in B-batch samples shows that the TKE spectra changes gradually from the amorphous kind to crystalline one with the increase of annealing time as shown in Fig. 2(a) [8]. That is, the TKE value is nearly independent of energy over 2.5 eV for as-quenched and the annealed sample for 20 minutes. This behavior is typical for Co-based amorphous alloys [6,7]. As annealing time increases, the shape of spectra curve does not gradually change. For the annealed samples over 5 hours, TKE value increases with energy up to 2.0 eV and is nearly constant up to 3.0 eV, and then shows a rapid increase. As a result, the spectra evolve into those of Co-based microcrystalline alloys [7,9]. These modifications of the TKE spectra for the annealed samples in air can be due to the change of microstructure in surface layer and appearance of microcrystalline phases.

The TKE value depends on the annealing field  $H_a$  as shown in Fig. 2(b). For the investigation of different fields for the annealed samples, TKE value has been found to change with the increase of magnetic field. In this case the

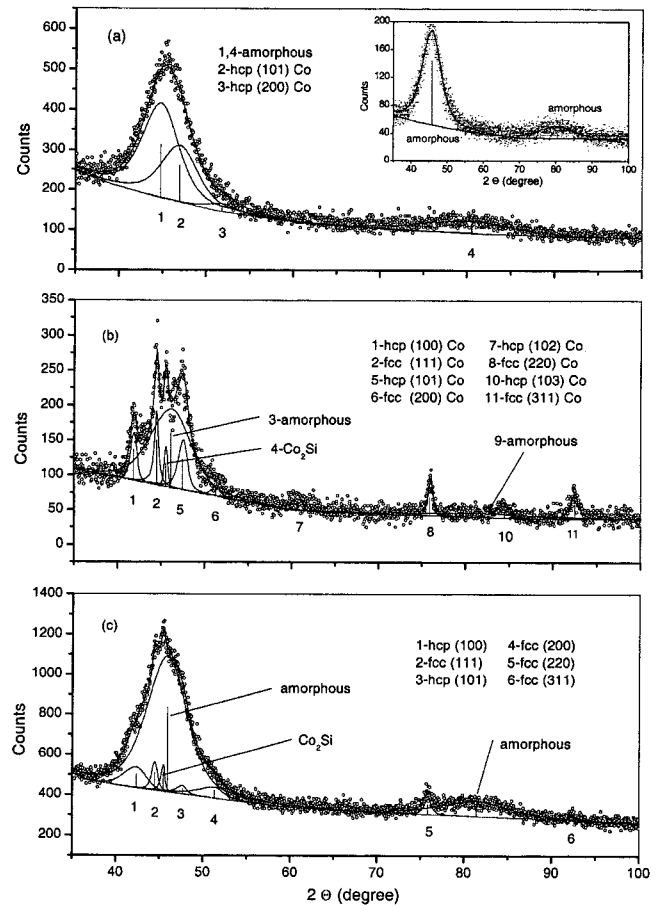


Fig. 3. GID-spectrum with incident angle  $\omega = 1^\circ$  in (a) annealed sample in vacuum (A-batch) and (b) in open air (B-batch) for 480 min, and (c) with  $\theta$ - $2\theta$  scan in B-batch for 480 min.

Table 1. Peak positions for annealed samples in vacuum (A-batch)

Annealing Parameters	Peak positions		
	$2\theta_1$	$2\theta_2$	$2\theta_3$
As-quenched	a-45.67	-	-
$T_a = 380\text{ }^\circ\text{C}$ , $t_a = 300\text{ min}$	45.05	46.9	50.96
$T_a = 380\text{ }^\circ\text{C}$ , $t_a = 480\text{ min}$	44.75	46.93	51.82

a- denotes the value of the position of amorphous peak.

spectra shape is stable and typical for the crystalline alloys.

The crystallization is more clearly shown in XRD measurement. Fig. 3(a), (b) present the  $2\theta$ -scan diffraction spectra (with incidence angle  $\omega = 1^\circ$ ) of A- and B-batch samples with  $t_a = 480\text{ min}$ , respectively. The penetration depth estimated from absorption law is about 300 nm [10]. The diffraction spectrum shows the typical amorphous state with two wide maxima for  $2\theta = 45.67^\circ$  and  $80.4^\circ$ , respectively, as shown in the insert of Fig. 3(a). Samples with shorter annealing times than 60 min show no distinctive changes between amorphous and A-batch annealed sam-

ples. However, the diffraction spectra, around the first maximum of amorphous state, of A-batch samples with  $t_a = 480\text{ min}$  (Fig. 3(a)) could be decomposed into three wide peaks centred around crystalline positions of hcp-Co, and around the amorphous phase. The peak positions for crystalline Co-phases are displayed in Table 1. The main peak  $2\theta_1$  is related to the amorphous phase. The peaks  $2\theta_2$  represent the main positions of initial nucleation of crystallisation to hcp-Co (101) phases, and  $2\theta_3$  position is probably related to the nucleation of hcp-Co (200).

The diffraction spectra in B-batch samples with short annealing time of  $t_a = 20$  and 40 min could be decomposed into five and nine, respectively, wide peaks centred around amorphous and crystalline positions of hcp- and fcc-Co, as summarized in Table 2. Samples annealed during long time of  $t_a = 300$  and 480 min (Fig. 3(b)) show very sharp peaks evidently connected with fcc-Co, hcp-Co and  $\text{Co}_2\text{Si}$  crystalline phases (see Table 3). From the compositional depth profile by Auger electron spectroscopy in the annealed samples in air, the B and Si atoms are diffused to the surface [5, 11]. The reduction of B and Si contents in underlying mate-

Table 2. Peak positions for annealed samples in air (B-batch)

Peak positions	$2\theta_1$	$2\theta_2$	$2\theta_3$	$2\theta_4$	$2\theta_5$	$2\theta_6$	$2\theta_7$	$2\theta_8$	$2\theta_9$
As-quenched	a-45.67	a-80.40							
$T_a = 380\text{ }^\circ\text{C}$ , $t_a = 20\text{ min}$	41.46	44.07	a-45.85	51.86	a-80.89				
$T_a = 380\text{ }^\circ\text{C}$ , $t_a = 40\text{ min}$	41.76	a-45.17	a-45.28	48.16	51.04	60.58	76.38	a-83.92	92.24

Table 3. Peak positions for annealed samples in air (B-batch)

Peak positions	$2\theta_1$	$2\theta_2$	$2\theta_3$	$2\theta_4$	$2\theta_5$	$2\theta_6$	$2\theta_7$	$2\theta_8$	$2\theta_9$	$2\theta_{10}$	$2\theta_{11}$
As-quenched	a-45.67	a-80.40									
$T_a = 380\text{ }^\circ\text{C}$ , $t_a = 300\text{ min}$	41.77	44.48	45.46	a-45.93	46.53	51.18	59.98	75.87	a-82.48	84.25	92.56
$T_a = 380\text{ }^\circ\text{C}$ , $t_a = 480\text{ min}$	41.85	44.42	45.52	a-45.81	47.55	51.31	60.74	75.93	a-82.65	84.39	92.49

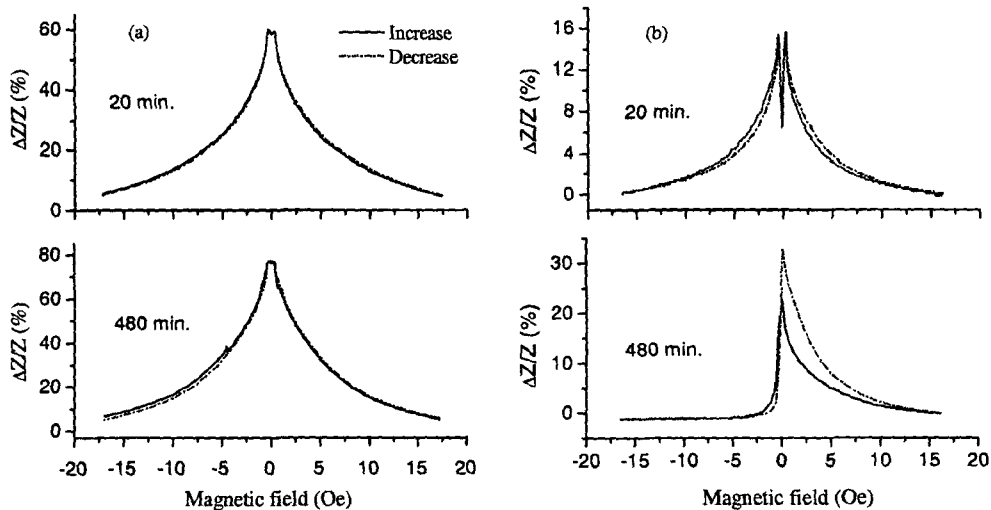


Fig. 4. GMI ratio profiles in (a) annealed sample in vacuum (A-batch) and (b) in open air (B-batch).

rial decreases the crystallization temperature of the depletion layer and thus, starts to nucleate fcc- and hcp-Co crystallites from 20 min annealing time.

In order to check how amorphous and crystalline phases are distributed in the depth of the ribbon, the incident beam angle of the X-ray was changed from  $\omega = 1^\circ$  to  $\omega = 5^\circ$ . In this measurement geometry, the structural information comes from the about  $1.5 \mu\text{m}$  thickness of the ribbon surface. The spectrum is changed drastically with the angle and the sharp crystalline peaks of surface have been dominated by greater amorphous fraction at  $\omega = 5^\circ$ . This effect, of course, is much stronger when the spectrum from  $\theta$ - $2\theta$  scan is taken for the analysis, as shown in Fig. 3(c). In this case structural information comes from the entire volume of a sample and contribution of amorphous fraction evidently dominates over surface crystalline phases fraction.

The GMI ratio profile in A-batch samples measured at 0.1 MHz is drawn in Fig. 4(a) for  $t_a = 20, 480$  min. The GMI profile shows one-peak behavior, irrespective of annealing time due to the dominant contribution of wall motion on transverse permeability. However, the GMI ratio increases with annealing time up to  $t_a = 480$  min.

For B-batch samples in Fig. 4(b), the GMI profile shows two-peaks for a  $t_a = 20$  min annealed sample. At 60 min, one of peaks disappears, and an asymmetric GMI profile exhibits a drastic step-like change near zero field for  $t_a \geq 300$  min. In other words, the peak in the antiparallel field region to annealing field decreases and shows the GMI-valve in parallel field region. However, there is hysteresis in the GMI-valve for increasing and decreasing fields. As the annealing time increase, hysteresis decreases and the on-set field of GMI-valve in 480 min annealed sample for increasing and decreasing fields nearly coincides with each other, as shown in Fig. 4(b). From these results, it is noted that the asymmetric GMI characteristics is related to the surface microstructures of fcc-Co, hcp-Co and  $\text{Co}_2\text{Si}$  crystalline phases.

#### 4. Conclusions

The magneto-optical investigation (TKE spectra) proves that the transformation of microstructure of near-surface layers in annealed amorphous  $\text{Co}_{66}\text{Fe}_4\text{B}_{15}\text{Si}_{15}$  samples is the result of annealing in air. However, the TKE spectra are typical one of amorphous alloys for the annealed samples in vacuum.

The XRD spectra for annealed samples in vacuum indicate atomic arrangements with initial nucleation of hcp-Co crystallite at  $380^\circ\text{C}$  annealing temperature. The samples

annealed in open air during short times for  $t_a \leq 40$  min show the formation of the initial surface nuclei of fcc- and hcp-Co crystalline phases. However, the XRD spectra in samples for long annealed time of  $t_a \geq 300$  min demonstrate sharp and well developed surface crystalline hcp-, fcc- Co and  $\text{Co}_2\text{Si}$  phases.

The difference of GMI profiles between vacuum and air annealed samples are distinctive for  $t_a \geq 300$  min. Even though the crystalline phase of hcp-Co is revealed in vacuum annealed samples for  $t_a \geq 300$  min in XRD measurement, the symmetric GMI profiles are dominated by an uniaxial anisotropy. However, the asymmetric GMI characteristics in annealed samples in air for  $t_a \geq 300$  min could be related to pronounced nucleation of hcp-Co, fcc-Co, and/or  $\text{Co}_2\text{Si}$  crystalline phases. However, the role of each crystalline phase in asymmetric GMI profiles remains unclear at present.

#### Acknowledgement

This work was supported by the Korea Research Foundation under Grand No. 1999-015-DP 0319.

#### References

- [1] L. V. Panina, K. Mohri, T. Uchiyama, M. Noda, K. Bushida, *IEEE Trans. Magn.* **34**, 1249 (1995).
- [2] G. V. Kurylanskaya, M. Vazquez, J. L. Munoz, D. Garcia, and J. McCord, *J. Magn. Magn. Mater.* **196-197**, 259 (1999).
- [3] X. L. Yang, J. X. Yang, G. Chen, G. T. Shen, B. Y. Hu, and K. Y. Jian, *J. Magn. Magn. Mater.* **175**, 285 (1997).
- [4] C. G. Kim, K. J. Jang, H. C. Kim, and S. S. Yoon, *J. Appl. Phys.* **85**, 5447 (1999).
- [5] K. J. Jang, C. G. Kim, S. S. Yoon, and K. H. Shin, *IEEE Trans. Magn.* **35**, 3880 (1999).
- [6] L. Valenichik, E. A. Ganshina, V. S. Guschin, D. N. Djuraev and G.S. Krinchik *Fiz. Met. Metalloved.* **67**, 1108 (1989).
- [7] L. Nikitin, L. Mironova, V. Litvintchev, and V. Katkevich *Fiz. Met. Metalloved.* **N2**, 92 (1991).
- [8] E. A. Ganshina, N. S. Perov, M. Yu. Kochneva, P. M. Sheverdyeva, C. G. Kim, and C. O. Kim, *ISPM 2001, AB-3*, submitted in *J. Magn. Magn. Mater.* (2001).
- [9] G. Krinchik, and V. Artemev *J. Eksp. Teor. Fiz.* **53**, 1901 (1967).
- [10] C. G. Kim, C. O. Kim, S. S. Yoon, T. Stobiecki, and W. Powroznik, submitted in *J. Magn. Magn. Mater.* (2001).
- [11] C. K. Kim, and R. C. O'Handley, *Mat. Sci. Eng.* **B38**, 16 (1996).